

## Observation of the dynamics leading to a conical intersection in dissociative electron attachment to water

D. J. Haxton,<sup>1</sup> H. Adaniya,<sup>1,2</sup> D. S. Slaughter,<sup>1</sup> B. Rudek,<sup>1,3</sup> T. Osipov,<sup>1</sup> T. Weber,<sup>1</sup> T. N. Rescigno,<sup>1</sup> C. W. McCurdy,<sup>1,4</sup> and A. Belkacem<sup>1</sup>

<sup>1</sup>*Lawrence Berkeley National Laboratory, Chemical Sciences, Berkeley, California 94720, USA*

<sup>2</sup>*Department of Applied Science, University of California, Davis, California 95616, USA*

<sup>3</sup>*J. W. Goethe Universität, D-60438 Frankfurt, Germany*

<sup>4</sup>*Departments of Applied Science and Chemistry, University of California, Davis, California 95616, USA*

(Received 8 June 2011; published 8 September 2011)

Following prior work on the lower-energy resonances, we apply techniques of momentum imaging and *ab initio* scattering calculations to the process of dissociative electron attachment to water via the highest-energy  $^2B_2$  resonance. We focus on the  $H^-$  anion fragment, which is produced via dynamics passing through and avoiding the conical intersection with the lower  $A_1$  state, leading to  $OH(^2\Pi)$  and  $OH(^2\Sigma)$ , respectively. The momentum imaging technique, when combined with theoretical calculations on the attachment amplitude and dissociation dynamics, demonstrates that the angular distributions provide a signature of the location of the conical intersection in the space of nuclear configurations.

DOI: [10.1103/PhysRevA.84.030701](https://doi.org/10.1103/PhysRevA.84.030701)

PACS number(s): 34.80.Ht

Conical intersections play diverse roles in chemistry and are one of the main avenues through which the coupling of nuclear and electronic motion proceeds in everyday molecules [1–3]. Dynamics on excited-state potential energy curves often involve conical intersections, which are ubiquitous for large molecules and highly excited states. Conical intersections are relevant to a variety of biologically and materially important processes, such as the absorption of light by chromophores [4,5].

The effect of conical intersections in providing a mechanism for the quenching of excited states has been long established [6–8], and numerous quantitative studies on their effect on branching ratios have been made [9–13]. There are many examples of studies that demonstrate manipulation of conical intersection dynamics, for instance in a pump-probe framework [5,14,15]. The measurement of angular distributions may permit the identification of the electronic symmetry or nuclear conformation of the initial state [12,13,16,17], as well as insight into the dissociation dynamics [18–23], in dissociating systems having a conical intersection.

A conical intersection between the  $^2B_2$  and  $^2A_1$  metastable states of the water anion was predicted [24] and demonstrated to be central to the dynamics following attachment to the  $^2B_2$  state [25,26]. Dissociative electron attachment (DEA) to the  $H_2O$  molecule proceeds via these and the  $^2B_1$  state at incident electron energies of approximately 12, 8.5, and 6.5 eV, respectively, and additionally in the condensed phase via a deep-valence state at approximately 25 eV [27]. The negative ion states subsequently fragment to produce the anions  $H^-$ ,  $O^-$ , and  $OH^-$ , in various arrangements [28–37]. Attachment to the  $^2B_2$  state leads to  $H^- + OH(^2\Sigma)$ , avoiding the conical intersection, or  $H^- + OH(^2\Pi)$ , passing through it.

Here, by combining calculations on the molecular-frame attachment amplitude with angular distributions obtained from experiment, we are able to confirm the location of a conical intersection in the space of nuclear geometries. The bending of the molecule to access the conical intersection leaves a clear imprint on the angular distributions for the  $OH$

( $X^2\Pi$ ) +  $H^-$  fragment. Our results are consistent with direct dissociation on the  $^2B_2$  state, avoiding the conical intersection, and bending by an additional  $15^\circ$  to access the lower  $OH(X^2\Pi)$  asymptote, going through the conical intersection. The angular distributions are therefore seen to directly reflect the bending dynamics required to transit the conical intersection and its location relative to the starting angle of  $104.5^\circ$ .

The experimental and theoretical methods employed here parallel those described in our previous publication [38]. In that work we provided a mechanistic study of the dynamics of DEA via the  $^2A_1$  state that demonstrated the coupled electronic and nuclear motion inherent to the process. The nuclear dynamics of dissociation was demonstrated to deviate markedly from the axial recoil approximation which provides the zeroth-order description to these dynamics via the analogy to a diatomic molecule, and the angular distributions were well reproduced by the method.

Our experimental approach will be described in detail in a separate paper and therefore only a general outline is presented here. A 50-kHz pulsed electron beam, produced by an electron gun, was directed to the interaction region, defined by the intersection of the electron beam and an effusive water vapor produced by a 0.5-mm-diameter stainless steel capillary directed at an angle of  $90^\circ$  to the electron gun. The electron pulse was typically 80 ns full width at half maximum (FWHM) and the electron energy resolution was found to be 0.8 eV FWHM, measured as twice the energy offset observed in achieving 50% of the peak ion yield at the sharp 6-eV  $H^-$  threshold for DEA to  $H_2O$ , compared with the high-resolution ion yield measurements of Fedor *et al.* [33]. The interaction region was centered between two large parallel electrodes separated by 15 mm. One electrode had a 1-mm aperture to transmit the molecular beam and was pulsed with a negative bias after the electron bunch exited the interaction region, driving negative ions through a grounded mesh in the opposing electrode and into the spectrometer, which was oriented at  $90^\circ$  with respect to the electron beam. Scattered electrons were prevented from entering the spectrometer by a uniform

dc magnetic field of typically 25 G, generated by a pair of Helmholtz coils that were oriented coaxially to the electron beam and confined it. The cylindrical spectrometer, based on the COLTRIMS [39] technique, consisted of 27 open copper electrodes with an acceleration region of 25 V/cm, a position-focusing lens, followed by a field-free drift region. The lens focused the two-dimensional (2-D) position image of the finite interaction region onto the detector, while the target spatial extent in the direction of the spectrometer axis was reduced by employing Wiley-McLaren time-focusing [40]. Negative ions were post-accelerated after the spectrometer to typically 500 eV before detection by a position-sensitive delay line detector. The entire spectrometer and detector assembly were housed in an aluminum cylindrical shield to further reduce the scattered electron background. A Computer Automated Measurement and Control (CAMAC) time to digital converter system collected the position and time of flight (TOF) data and the raw data were stored in list mode format for offline analysis.

The ion spectrometer collects the full  $4\pi$  sphere of dissociating anions while actively discriminating against electrons. Negative ions originating from residual background gas are removed in offline analysis by mass and ion kinetic energy selection. The three-dimensional momentum images of the ionic fragment, determined from the final ion position on the detector and TOF, yield a kinematically complete picture of two-body dissociation and permit the discrimination of three-body breakup events. A typical  $\text{H}^-$  momentum distribution for the  ${}^2B_2$  resonance is shown in Fig. 1. Three distinct rings are clearly resolved, each illustrating a different dissociation pathway leading to different ion momenta. We can clearly determine the internal energy of the OH fragment from the kinetic energy release: the outermost ring corresponds to the  $\text{H}^-$  and  $\text{OH}({}^2\Pi)$ , while the second ring is due to  $\text{H}^-$  and  $\text{OH}({}^2\Sigma)$  and the innermost band is the result of three-body breakup.

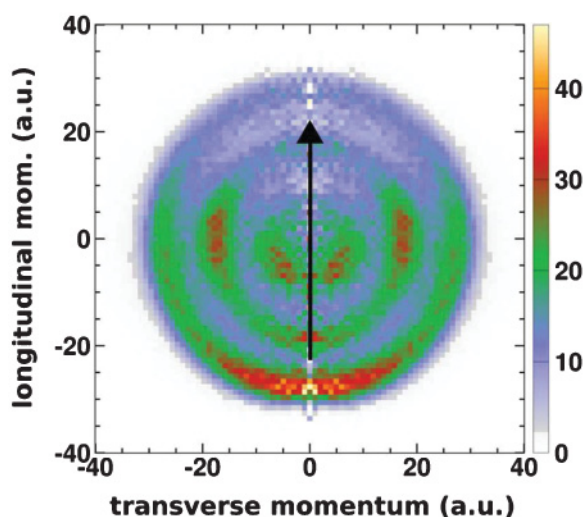


FIG. 1. (Color online) Experimental COLTRIMS image of  $\text{H}^-$  fragments from attachment at 11.3 eV. The transverse and longitudinal momentum in atomic units relative to the incident electron are plotted along the abscissa and ordinate, respectively, with the incident electron traveling bottom (backward) to top (forward).

In order to make a connection between the laboratory-frame experimental observations and the dynamics in the body frame, we use a combination of quantum-mechanical calculations of the body-frame attachment amplitude [41] and classical trajectory calculations on complex-valued potential energy surfaces [25]. Autoionization on the complex-valued potential energy surfaces is accounted for stochastically via a survival probability at each time step,  $\exp[-\Gamma(\vec{R})\Delta t]$ , where  $\Gamma(\vec{R})$  is the width of the resonance in the Born-Oppenheimer approximation. The present calculations employ Tully's fewest switches method [42] to incorporate the effect of the conical intersection between the  ${}^2B_2$  and  ${}^2A_1$  states.

The trajectories shown in Fig. 2 appear to recoil along straight lines in the asymptotic region. They show a clear signature of the effect of the conical intersection upon the angular distribution in the molecular frame. The conical intersection occurs at small bond angles, from approximately  $65^\circ$  to  $85^\circ$ , as shown in Fig. 3. As a result, the trajectories avoiding the conical intersection to  $\text{H}^- + \text{OH}({}^2\Sigma)$ , shown in the top panel of Fig. 2, recoil at an angle of approximately  $45^\circ$  in the molecular frame, whereas those which pass through it, leading to  $\text{H}^- + \text{OH}({}^2\Pi)$ , are emitted at approximately  $30^\circ$  degrees, relative to the initial  $57.24^\circ$ .

In Fig. 4 we show the correlation between the molecular-frame momentum angle at the transition through the conical intersection and the final angle of recoil, as calculated with the surface hopping method. The correlation between the direction of momentum at the conical intersection crossing and the asymptotic direction is indeed good, with  $R^2 = 0.863$ , and thus we see that the final recoil angle is a faithful proxy for the angle at which the molecule traverses the conical intersection.

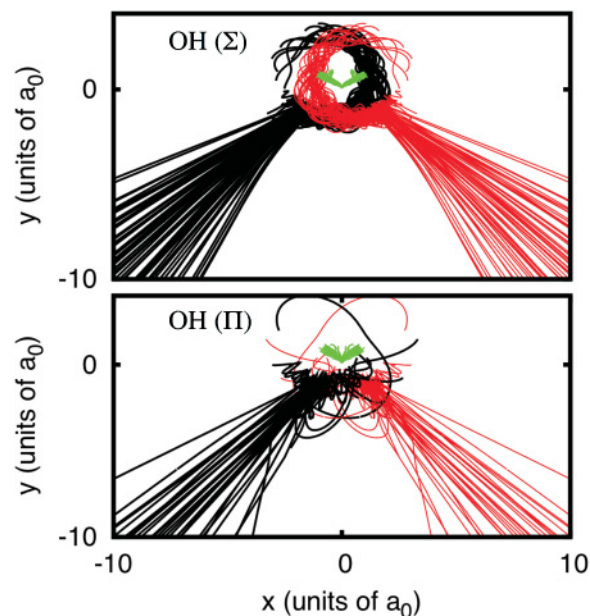


FIG. 2. (Color online) Trajectories leading through (bottom) and avoiding (top) the conical intersection, in the space-fixed frame. The molecule starts at the top of the figure and the paths of the oxygen (light gray; green online; staying near the origin) and two hydrogen atoms (black and dark gray; black and red online) are plotted for an ensemble of trajectories.

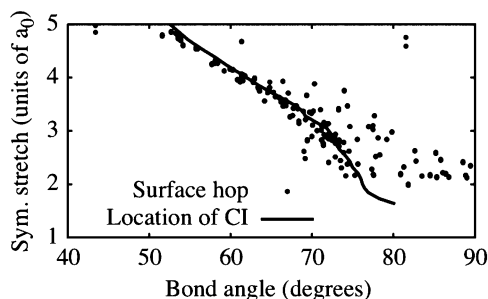


FIG. 3. Location of the  ${}^2B_2\text{-}{}^2A_1$  conical intersection (line), which occurs at equal bond lengths  $r_1 = r_2$ , and location of surface hops (points) as functions of symmetric stretch coordinate and bond angle.

In the bottom panel of Fig. 5 we show the experimental results for the laboratory-frame angular distribution for production of OH ( ${}^2\Sigma$ ) (gray triangles), avoiding the conical intersection, and OH ( ${}^2\Pi$ ) (black dots), passing through the conical intersection. These are determined directly from the ion momentum distribution integrated over each kinetic energy peak corresponding to the bands in Fig. 1 due to two-body dissociation.

We may understand these distributions by examining the probability of electron attachment as a function of angle of incidence in the molecular frame. This probability is the square of the entrance amplitude [43], labeled  $V_a$ ;  $V_a(\theta, \phi; \vec{R}) = \langle \Psi^-(\theta, \phi; \vec{R}) | H | \varphi \rangle$ , where  $\Psi^-$  is a background scattering state with incident wave at angles  $\theta, \phi$ , and  $\varphi$  is a discrete approximation to the resonance state. If  $\phi$  is the azimuthal angle about the recoil axis, and the variation with respect to  $\vec{R}$  can be neglected (the constant-eigenmode approximation), then the prediction for the observed angular distribution is [43]  $\int d\phi |V_a(\theta, \phi)|^2$ .

In the top panel of Fig. 5 we show the entrance amplitude  $V_a(\theta, \phi)$  in the molecular frame at the equilibrium geometry of the neutral and the axial recoil prediction for the angular dependence given this entrance amplitude. The entrance amplitude is peaked along the OH bonds, favoring attachment by electrons incident in these directions. The axial recoil prediction shows two peaks, at approximately  $90^\circ$  and  $180^\circ$ , in the perpendicular and backward directions. With reference to the entrance amplitude in the inset of this figure, these two peaks may be understood as resulting from attachment

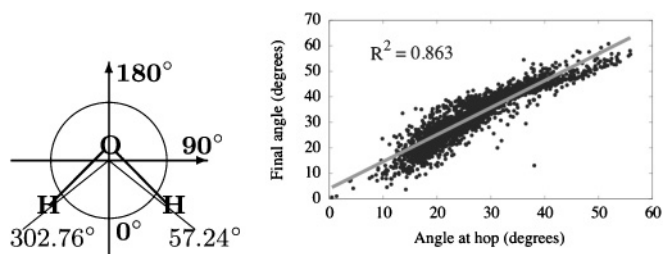


FIG. 4. Left: Definition of molecular-frame angles relative to the center of mass. Right: In terms of these angles, there is a strong correlation between the direction of the space-fixed momentum vector upon transit through the conical intersection and its final direction. The final recoil as a function of the angle of crossing is shown as black dots; the best linear fit is the gray line.

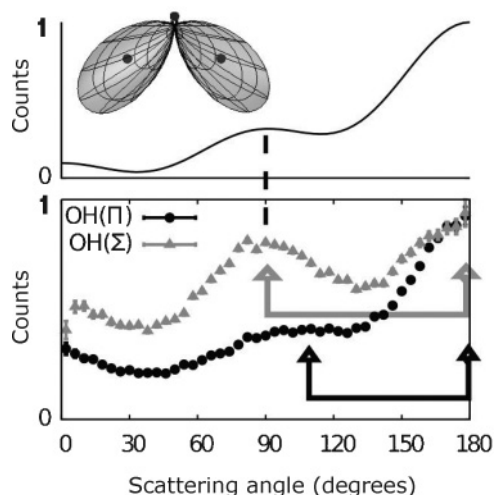


FIG. 5. Top: Entrance amplitude  $V_a$  as a function of polar angle in the molecular frame, and axial recoil prediction for the laboratory-frame  $H^-$  angular distribution as a function of scattering angle from the  ${}^2B_2$  resonance. Bottom: Experimental angular distributions of  $H^-$  fragments (dots) corresponding to  $H^- + OH$  ( ${}^2\Sigma$ ) (gray triangles) and  $H^- + OH$  ( ${}^2\Pi$ ) (black circles) at 11.3 eV. Error bars indicate one standard deviation. The intensity scales are linear and have arbitrary units and the arrows and dashed line are intended to guide the eye and are referred to in the text.

and dissociation along different and the same OH bonds, respectively.

The experimental results in the bottom panel of Fig. 5 also show two peaks in the angular distribution, marked with gray and black arrows. The dissociation dynamics of this highly excited metastable state is different from the axial recoil prediction, also shown in Fig. 5. The backward ( $180^\circ$ ) peak is suppressed in the experiment; this feature will be discussed in subsequent work.

We focus on the position of the two peaks. The difference in peak locations is highlighted by arrows in the bottom of Fig. 5. One can see that the peaks occur farther apart for production of  $H^- + OH$  ( ${}^2\Sigma$ ), avoiding the conical intersection (gray triangles), than for production of  $H^- + OH$  ( ${}^2\Pi$ ), passing through the conical intersection (black dots). For the former, the positions of the peaks at approximately  $90^\circ$  and  $180^\circ$  scattering angle comport with the axial recoil prediction shown in the top panel of Fig. 5. As shown by the dashed line in Fig. 5, the perpendicular peak occurs at the same scattering angle as predicted by the axial recoil approximation. This similarity between the axial recoil prediction and the experimental results for OH ( ${}^2\Sigma$ ) is consistent with dissociation in which the bond angle changes relatively little, tending to avoid the conical intersection. For OH ( ${}^2\Pi$ ) (black dots), passing through the conical intersection, the bond angle must decrease and as a consequence the perpendicular peak is shifted backward and the backward peak is shifted forward somewhat by this scissoring motion concomitant with dissociation and passage through the conical intersection. The classical trajectory calculations indicate that the observed recoil angle does indeed reflect the angle of passage through the conical intersection and therefore eliminate the possibility that the observed differences

are due to different dynamics beyond the range of the conical intersection. Therefore, the experimental results corroborate the position of the conical intersection, occurring at small bond angles relative to the  $104.5^\circ$  starting point, calculated in Ref. [25].

In conclusion, we have demonstrated that the observed variations in the final-state angular dependence for  $\text{H}^-$  production via dissociative attachment to the  $^2B_2$  Feshbach resonance of the water anion are a clear signature of the dynamics either passing through or avoiding the conical intersection. This conical intersection lies at small bond angles and is

imaged via the closing of the angle between of the two peaks seen in the experimental angular distributions. The use of molecular-frame calculations on the attachment probability permits this connection between the observed features and the dynamics of dissociation.

This work was performed under the auspices of the US Department of Energy by LBNL under Contract No. DE-AC02-05CH11231 and was supported by the US Department of Energy, Office of Basic Energy Sciences, Division of Chemical Sciences.

- 
- [1] D. Yarkony, *Rev. Mod. Phys.* **68**, 985 (1996).  
 [2] M. Baer, *Phys. Rep.* **358**, 75 (2002).  
 [3] G. A. Worth, *Annu. Rev. Phys. Chem.* **55**, 127 (2004).  
 [4] A. Virshup, C. Punwong, T. Pogorelov, B. A. Lindquist, C. Ko, and T. Martinez, *J. Phys. Chem. B* **113**, 3280 (2009).  
 [5] S. Logunov, V. Volkov, M. Braun, and M. El-Sayed, *Proc. Natl. Acad. Sci. USA* **98**, 8475 (2001).  
 [6] H. Krautwld, L. Schneider, K. Welge, and M. Ashfold, *Faraday Discuss. Chem. Soc.* **82**, 99 (1986).  
 [7] T. Martinez, *Chem. Phys. Lett.* **272**, 139 (1997).  
 [8] S. A. Harich, X. Yang, X. Yang, and R. N. Dixon, *Phys. Rev. Lett.* **87**, 253201 (2001).  
 [9] M. Abe, Y. Ohtsuki, Y. Fujimura, Z. Lan, and W. Domcke, *J. Chem. Phys.* **124**, 224316 (2006).  
 [10] A. Hoffmann and R. de Vivie-Riedle, *J. Chem. Phys.* **112**, 5054 (2000).  
 [11] B. C. Hoffman and D. R. Yarkony, *J. Chem. Phys.* **113**, 10091 (2000).  
 [12] G. Waschewsky, P. Kash, T. Myers, D. Kitchen, and L. Butler, *J. Chem. Soc., Faraday Trans.* **90**, 1581 (1994).  
 [13] A. Eppink and D. Parker, *J. Chem. Phys.* **109**, 4758 (1998).  
 [14] H. Kang, B. Jung, and S. Kim, *J. Chem. Phys.* **118**, 6717 (2003).  
 [15] L. Seidner, G. Stock, A. Sobolewski, and W. Domcke, *J. Chem. Phys.* **96**, 5298 (1992).  
 [16] W. McGivern, R. Li, P. Zou, and S. North, *J. Chem. Phys.* **111**, 5771 (1999).  
 [17] P. Kash, G. Waschewsky, R. Morss, L. Butler, and M. Franci, *J. Chem. Phys.* **100**, 3463 (1994).  
 [18] G. Amaral, K. Xu, and J. Zhang, *J. Chem. Phys.* **114**, 5164 (2001).  
 [19] G. Waschewsky, D. Kitchen, P. Browning, and L. Butler, *J. Phys. Chem.* **99**, 2635 (1995).  
 [20] J. Wei, A. Kuczmann, J. Reidel, F. Renth, and F. Temps, *Phys. Chem. Chem. Phys.* **5**, 315 (2005).  
 [21] D. Mordaunt, M. Ashfold, and R. Dixon, *J. Chem. Phys.* **109**, 7659 (1998).  
 [22] J. Liu, F. Wang, H. Wang, B. Jiang, and X. Yang, *J. Chem. Phys.* **122**, 104309 (2005).  
 [23] S. Harich, X. Yang, D. Hwang, J. Lin, X. Yang, and R. Dixon, *J. Chem. Phys.* **114**, 7830 (2001).  
 [24] D. J. Haxton, T. N. Rescigno, and C. W. McCurdy, *Phys. Rev. A* **72**, 022705 (2005).  
 [25] D. J. Haxton, C. W. McCurdy, and T. N. Rescigno, *Phys. Rev. A* **75**, 012710 (2007).  
 [26] D. J. Haxton, T. N. Rescigno, and C. W. McCurdy, *Phys. Rev. A* **75**, 012711 (2007).  
 [27] G. A. Kimmel and T. M. Orlando, *Phys. Rev. Lett.* **77**, 3983 (1996).  
 [28] N. B. Ram, V. S. Prabhudesai, and E. Krishnakumar, *J. Phys. B* **42**, 225203 (2009).  
 [29] P. Rawat, V. S. Prabhudesai, G. Aravind, N. Bhargavaram, M. A. Rahman, and E. Krishnakumar, *J. Phys.: Conf. Ser.* **80**, 012018 (2007).  
 [30] P. Rawat, V. S. Prabhudesai, G. Aravind, M. A. Rahman, and E. Krishnakumar, *J. Phys. B* **40**, 4625 (2007).  
 [31] E. Krishnakumar, V. S. Prabhudesai, and N. B. Ram, *J. Phys.: Conf. Ser.* **88**, 012073 (2007).  
 [32] V. S. Prabhudesai, D. Nandi, and E. Krishnakumar, *J. Phys. B* **39**, 277 (2006).  
 [33] J. Fedor *et al.*, *J. Phys. B* **39**, 3935 (2006).  
 [34] D. S. Belic, M. Landau, and R. H. Hall, *J. Phys. B* **14**, 175 (1981).  
 [35] R. N. Compton and L. G. Christophorou, *Phys. Rev.* **154**, 110 (1967).  
 [36] C. E. Melton, *J. Chem. Phys.* **57**, 4218 (1972).  
 [37] D. J. Haxton, T. N. Rescigno, and C. W. McCurdy, *Phys. Rev. A* **78**, 040702 (2008).  
 [38] H. Adaniya, B. Rudek, T. Osipov, D. J. Haxton, T. Weber, T. N. Rescigno, C. W. McCurdy, and A. Belkacem, *Phys. Rev. Lett.* **103**, 233201 (2009).  
 [39] R. Dörner, V. Mergel, O. Jagutzki, L. Spielberger, J. Ullrich, R. Moshhammer, and H. Schmidt-Böcking, *Phys. Rep.* **330**, 95 (2000).  
 [40] W. C. Wiley and I. H. McLaren, *Rev. Sci. Inst.* **26**, 1150 (1955).  
 [41] D. J. Haxton, C. W. McCurdy, and T. N. Rescigno, *Phys. Rev. A* **73**, 062724 (2006).  
 [42] J. Tully, *J. Chem. Phys.* **93**, 1061 (1990).  
 [43] T. F. O'Malley and H. S. Taylor, *Phys. Rev.* **176**, 207 (1968).